2016

Modeling Reciprocating Compressors Using A Cartesian Cut-Cell Method With Automatic Mesh Generation

David Henry Rowinski
Convergent Science, Inc., United States of America, david.rowinski@convergecfd.com

Kenneth Edward Davis
Convergent Science, Inc., United States of America, kenneth.davis@convergecfd.com

Modeling Reciprocating Compressors Using A Cartesian Cut-Cell Method With Automatic Mesh Generation

David ROWINSKI*, Kenneth DAVIS

Convergent Science, Inc.
Madison, WI, USA
david.rowinski@convergecfd.com

* Corresponding Author

ABSTRACT

Computational Fluid Dynamics (CFD) models can offer great insight into flow phenomena and complex fluid-structure interactions present in reciprocating compressors. This is often achieved, however, at large computational cost and considerable user setup time. In this study, a Cartesian cut-cell finite-volume method is applied to model a small displacement refrigeration compressor. The cut-cell method has the key feature of representing discrete cell volumes exactly without requiring the computational grid to coincide with the bounding geometry. Additionally, the grid is dynamically generated at each time step based on the instantaneous boundary positions and is automatically refined based on gradients of local flow variables. These two features make this method ideal for modeling the deformation of the valves, the motion of the piston, and the complex geometries of the suction and discharge mufflers. The model is validated against experimental data. The sources of numerical error in the model are assessed, including the spatial and temporal discretization error and the model treatment for valve opening, closure, and contact. Lastly, several automated grid generation strategies are presented to establish guidelines for balancing cost and accuracy. The model formulation highlights the ease of incorporating complex and moving geometries characteristic of reciprocating compressors into a CFD model at a reasonable cost.

1. INTRODUCTION

Understanding the nature of the flows in reciprocating compressors is vital in engineering work involving their design and analysis. While models of various levels of complexity have been developed, three-dimensional time-accurate computational fluid dynamics (CFD) provides some key advantages. These advantages include the identification of flow structures important to viscous losses, local heat transfer, mixing, and the elucidation of the interaction of the flow with the geometry. Furthermore, these models are more complete in the sense that they are mostly free from empirical corrections which may be valid over small ranges of operating conditions. As Prasad (2004) points out in his review, though reciprocating compressors are typically viewed as thermodynamic devices, most of the important losses are fluid dynamic in nature, making understand the flow of critical importance.

Over the last twenty years, considerable advancement has been made in the application of CFD models to reciprocating compressors. Cyklis (1994) applied a commercial CFD package to model two-dimensional flow through a suction valve. Fagotti and Possamai (2000) applied commercial CFD tools to model flows in compressor components, and noted that one important aspect of the problem setup was the user selection of grid size. Ottitsch (2000) applied CFD to model a variety of different valve types in steady state incompressible flow. Chikurde (2002) presented an analysis of a full compressor geometry and noted that it was critical to apply sufficient grid resolution in regions of important flow features. In addition, complex flow features such as rivets and fillets were removed to simplified the meshing procedure. In more recent studies, Kim (2006) applied two-way coupled fluid-structure interaction (FSI) to model the behavior of valves, and Pereira (2007) applied CFD to model the full three-dimensional domain of a refrigeration compressor. Pereira (2008) compared models of various levels of complexity and found advantage of the CFD's predictive nature, despite finding the three-dimensional model costs too high for use in optimization. Mistry (2012) and Rigola (2012) explored three-dimensional modeling of the flow over valves,

among other topics such as turbulence model effects. Rodrigues (2014) applied a variety of turbulence models to full three-dimensional compressor models.

One of the major limitations to the adoption of CFD in the routine design and analysis process for reciprocating compressors has been the bottleneck of grid generation, as pointed out by Prasad (2004) and others. Reciprocating compressors typically feature complex geometries in the suction and discharge mufflers, as well as moving parts of the piston and valves. Furthermore, the types of valves and other moving parts used may vary widely between different reciprocating compressor types, especially when prototyping new design concepts.

In this study, an alternate approach to modeling reciprocating compressors is presented. The majority of previous works on CFD studies of reciprocating compressors have featured models requiring the construction of a numerical grid. Here the authors present the use of a Cartesian cut-cell method in which the grid is dynamically generated at every time step based on exact and instantaneous geometry definition. The purpose of this work is to investigate the numerical accuracy of this cut-cell based method, specifically in its application to modeling reciprocating compressors.

2. METHODOLOGY

The Cartesian cut-cell method described by Senecal et al. (2007) is employed in this work. The model begins from a triangulated surface which describes the volume of a computational domain. The volume is filled by an orthogonal base grid of a user-specified size. Wherever the triangulated surface intersects the base grid, the base grid cells are cut into arbitrary sided polyhedra. Thus the volume represented in the cut-cells is exactly the same as the volume of the original triangulated surface, independent of the base grid size used. Because the process of forming the mesh is entirely automatic, it can easily accommodate complex boundary shapes and complex boundary motion without any user intervention. Because the method is based on standard orthogonal grids, it is computationally simple and demonstrates good numerical stability.

The conservation equations are solved using the finite-volume method. All values in the model are collated at the center of the computational cells. The algorithm of Rhie and Chow (1983) is used to prevent checker-boarding in the velocity and pressure fields. In the present study, second-order spatial discretization is used for solving all the conservation equations. To maintain stability, the time accuracy is set to a fully implicit first-order scheme for this work. The transport equations are solved using a modified Pressure Implicit with Splitting of Operators (PISO) method from Issa (1985). A variable time-step approach is used to ensure stability and to increase the time step when possible. The time step is controlled through the Courant-Friedrichs-Lewy (CFL) numbers based on local cell sizes, velocity, speed of sound, and diffusivity. Turbulence is modeled using the RNG k-epsilon model of Yahkot (1986) with standard model constants.

All simulations are run in parallel using Message Passing Interface (MPI). The automatic domain decomposition technique of Karypis (2013) is used to control the load balance, which is not trivial for this method. Because of change to the computational volume over time (for example, by moving boundaries), or addition of cells through Automatic Mesh Refinement (AMR), there may be a significant non-uniformity to the distribution of cells in space.

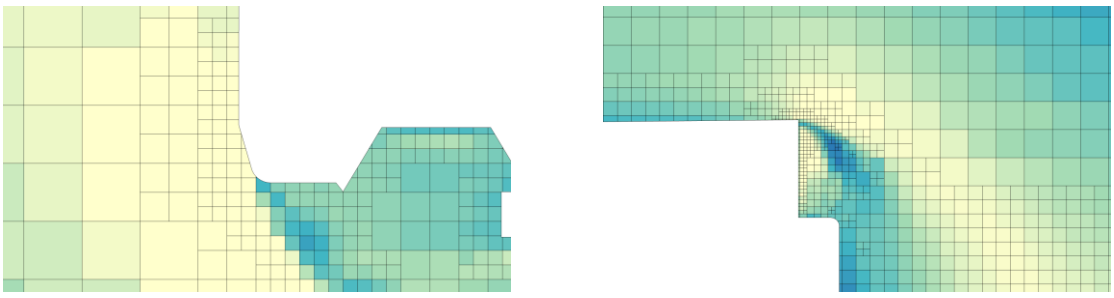

Figure 1: (Left) A cut-plane showing the base grid cells, far to the left, and the smaller embedded cells which are cut by the boundary into arbitrary sided polyhedra. (Right) A cut-plane showing smaller cells which have been created automatically through a refinement based on the curvature of instantaneous field variable values.

It is essential to ensure that the grid resolution at any location is sufficiently small to have minimal impact on the solution of the flow field. In most cases, it is very difficult to determine beforehand the locations and times over which a finer grid resolution is required. Automatic Mesh Refinement (AMR) is employed in these models to provide a way to handle this problem, as demonstrated in Figure 1. Ideally, a good AMR method should add the cells where the simulation is most under-resolved, or where the sub-grid scale variation of a field variable is the largest. As shown by Pomraning (2000) and others, any sub-grid scalar field can be expressed as a series sum. So here, the refinement criteria are based on the instantaneous curvature of the solution fields, or the first term in the series for the sub-grid scale term.

The equation of state used in this study is that of Peng and Robinson (1976), in which the critical temperature, critical pressure, and acentric factor of the working fluids must be provided. The standard departure functions described by Poling (2001) are used to compute real-gas properties for enthalpy, entropy, and specific heat capacity. The transport properties of viscosity and conductivity are described as tabulated functions of temperature and pressure based on the data provided by Perkins (2000) and Tillner-Roth (1994).

In this particular study, moving and deforming solids are incorporated into the model using an explicit solid-fluid coupling scheme. The classical Euler-Bernoulli beam equation as described by Timoshenko (1953), is discretized over the length of the solid reeds. A finite-difference scheme is used to determine the local beam velocity and displacement. The scheme is spatially second-order accurate, and first-order accurate in time through a fully implicit solution in time. The local pressure and viscous forces over the solid are evaluated and fed into the beam equation as a spatially varying load. The model can account for variation in the cross-section area, density, thickness, elastic modulus, and moment of inertia across the length of the beam. The model assumes the beam is subject to lateral loads only and that the displacement is small. To handle contact along the beam, an implicit penalty force method is used. If contact is determined, the time step is re-evaluated with a force applied constraining the node displacement.

3. TEST CASE DESCRIPTION

The method described has been used often in the modeling of internal combustion engines, for example by Senecal (2007) and Pomraning (2014). This application area shares several important similarities and differences from the application presented here. In this section, the physical test case studied in this work is described, the computational model inputs are presented, and the numerical test cases are outlined.

3.1 Description of Physical Compressor Studied

The compressor studied in this work is a 13.0 cubic centimeter displacement hermetic refrigeration compressor. All information, including the geometry, operating conditions, and experimental data has been provided to the authors. The working fluid is R-134a. The geometry consists of the components shown in Figure 2, and extends from the input of the suction muffler to the end of the discharge line. The operating conditions for the case considered here is a low back pressure (LBP) with a condensing temperature of 54°C. The nominal speed of the compressor is 3000 revolutions per minute (RPM). The cylinder pressure is measured, as are the lifts of the suction and discharge reeds.

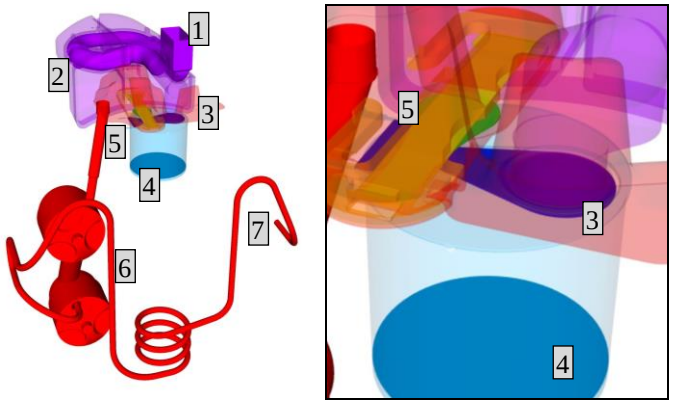

Components of Compressor Assembly in CFD Model
1. Inflow
2. Suction Muffler and Port
3. Valve Plate and Suction Reed Gasket
4. Piston
5. Discharge Reed, Booster, and Limiter
6. Discharge Muffler and Lines
7. Outflow

Figure 2: The geometry of the test case compressor.

3.2 Computational Model Setup

The computational model is constructed first by extracting a wetted surface geometry of the compressor components in contact with the working fluid. This surface contains all the necessary information concerning the geometry. The suction muffler inlet is set as a total pressure inflow boundary condition, and the measured temperature at that inlet as well. At the discharge line outlet, the discharge pressure is set as a static pressure boundary condition. At the walls, standard two-layer law-of-the-wall models are used for velocity and temperature, and a measured wall temperature is used around the cylinder to model the heat transfer.

The motion of the piston is set according to a standard crank-slider mechanism using the geometric parameters of the compressor's crankshaft, connecting rod, and wrist pin offset. The motion of the suction valve, discharge valve, and discharge booster are set according to the beam model mentioned in Section 2. The authors emphasize that all these boundary motions are easily incorporated into the model without the need for any user intervention concerning how the motion will affect the computational grid.

4. Results and Discussion

As the purpose of this work is to ascertain the numerical errors in the Cartesian cut-cell model, a number of test cases are performed to target specific parts of the model which may be prone to numerical error. First, a base case is run using an intermediate grid resolution. Those calculations begin at bottom dead center with the cylinder region initialized at the conditions of the suction muffler. The model is run until cyclic convergence is reached. Figure 3 shows the cooling capacity (normalized by the measured cooling capacity), and the power (normalized by the measured power) for the last three cycles. As can be seen from the data, there is less than 1% variation in these measures by the third cycle. The pressure-volume (PV) diagram is shown in Figure 3 for the last three cycles. In this figure, the pressure is normalized to P^* by the difference between suction and discharge pressures, so that the normalized pressure, P^*, is zero at suction conditions and unity at discharge. The volume is also normalized to V^* by the displacement.

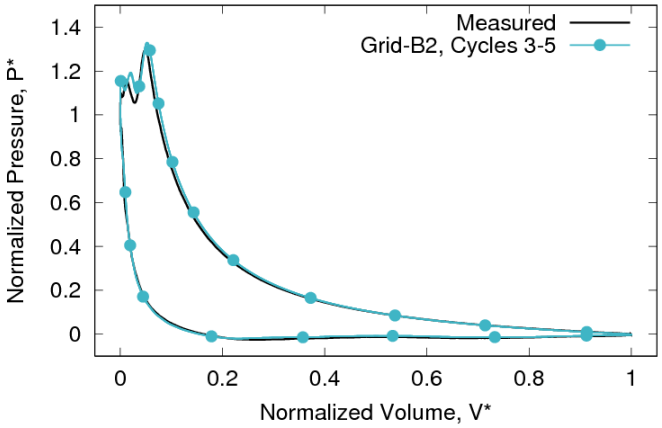

Case	Norm. Cooling Capacity	Norm. Power (Point)	Norm. Power (Mean)
Measured	1	1	N/A
Model, Cycle #3	0.994	1.019	1.037
Model, Cycle #4	0.992	1.019	1.037
Model, Cycle #5	0.995	1.020	1.038

Figure 3: PV Diagram (left) for base case for cycles three to five along with experimental measurements, and table (right) of normalized cooling capacity and power statistics.

4.1 Effects of the spatial accuracy of the model

Once cyclic convergence is reached, a series of grid resolution studies are performed for both suction and discharge events. These simulations begin approximately 20 degrees before the valves open, and are initialized with conditions from the previous model. The authors note that each grid resolution study is performed by changing just a single set of parameters in the model inputs. For two of the grids, Grid-A0 and Grid-B0, there is no automatic mesh refinement (AMR) activated. For the remaining grids, AMR is activated with various levels of refinement allowed. An AMR scale value means that cells are allowed to be divided recursively by that number of times. (For example, a scale of 2 means that a base grid cell can be subdivided into eight grid cells, which can again be divided into a total of sixty-four grid cells.) The details of all seven grids studied are shown in Table 1.

Table 1: Details about the seven grids used in the various grid refinement studies.

Grid Name	Number of Base Grid Cells Across Bore	AMR Scale	Base Grid Size (mm)	Finest Grid Size (mm)	Max Cell Count (MCell)
Grid-A0	10	0	2.6	0.65	0.047
Grid-B0	20	0	1.3	0.33	0.18
Grid-B2	20	2	1.3	0.33	0.24
Grid-B3	20	3	1.3	0.16	0.48
Grid-C2	40	2	0.65	0.16	1.3
Grid-C3	40	3	0.65	0.08	2.1
Grid-C4	40	4	0.65	0.08	6.3

To compare the cases, two additional metrics are introduced: Y^*, the delivered mass fraction, and M^*, the normalized mass flow rate. For the suction event, Y^* is the mass fraction of fresh suction gas in the cylinder, and M^* is the mass flow rate into or out of the cylinder normalized by the characteristic mass flow rate, defined by the mass at suction conditions occupying the displacement volume per time length of a cycle. For the discharge event, Y^* is defined as the mass in the discharge port which originated from the cylinder, normalized by the mass of the cylinder prior to discharge. These quantities are all tracked in simulation by solving transport equations for two additional passive scalars.

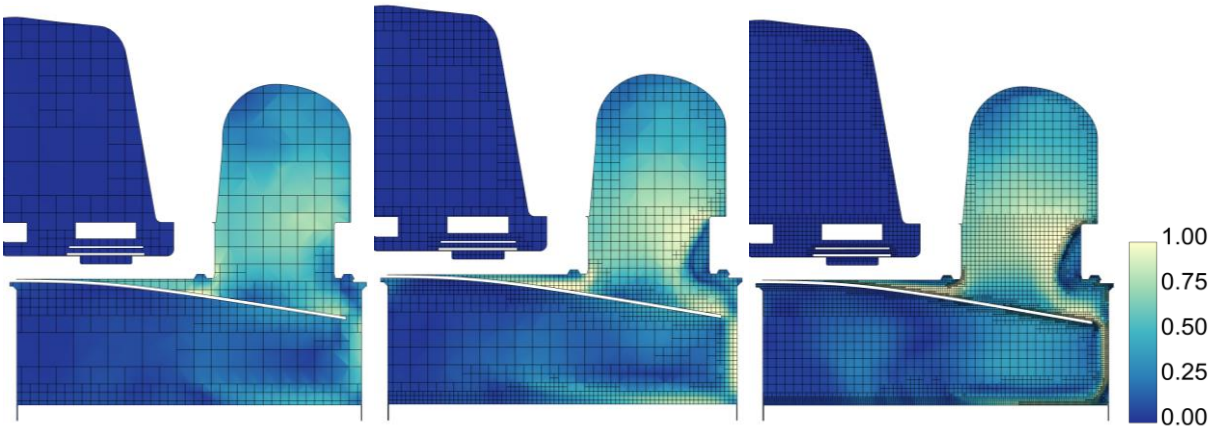

Figure 3: Cut-planes along the center of the suction reed, colored by normalized velocity for three of the grids studied. From left to right, the grids are Grid-A0, Grid-B2, and Grid-C3.

Three representative grids from the suction event grid refinement studies are shown in Figure 3. In the leftmost figure is Grid-A0, the coarsest grid with no AMR. In the center figure is the intermediate Grid-B2. One of the finest grids is shown to the right. As can be seen from the figure, AMR adds the cells in the regions where the critical flow structures are present.

The grid resolution study for the suction process showed relatively little sensitivity of either M^* or Y^* on all but the coarsest grid. The results were encouraging in that they indicated numerical grid convergence of the solution on relatively coarse meshes. The error between the measured values and the modeled values is far greater than the grid discretization error on the finest six grids. Figure 4 shows the PV diagram, the suction reed lift (normalized by the valve length), and the mass flow rates for four of the grids. The similarity in the solution for the six finest grids can be seen in all four of these plots.

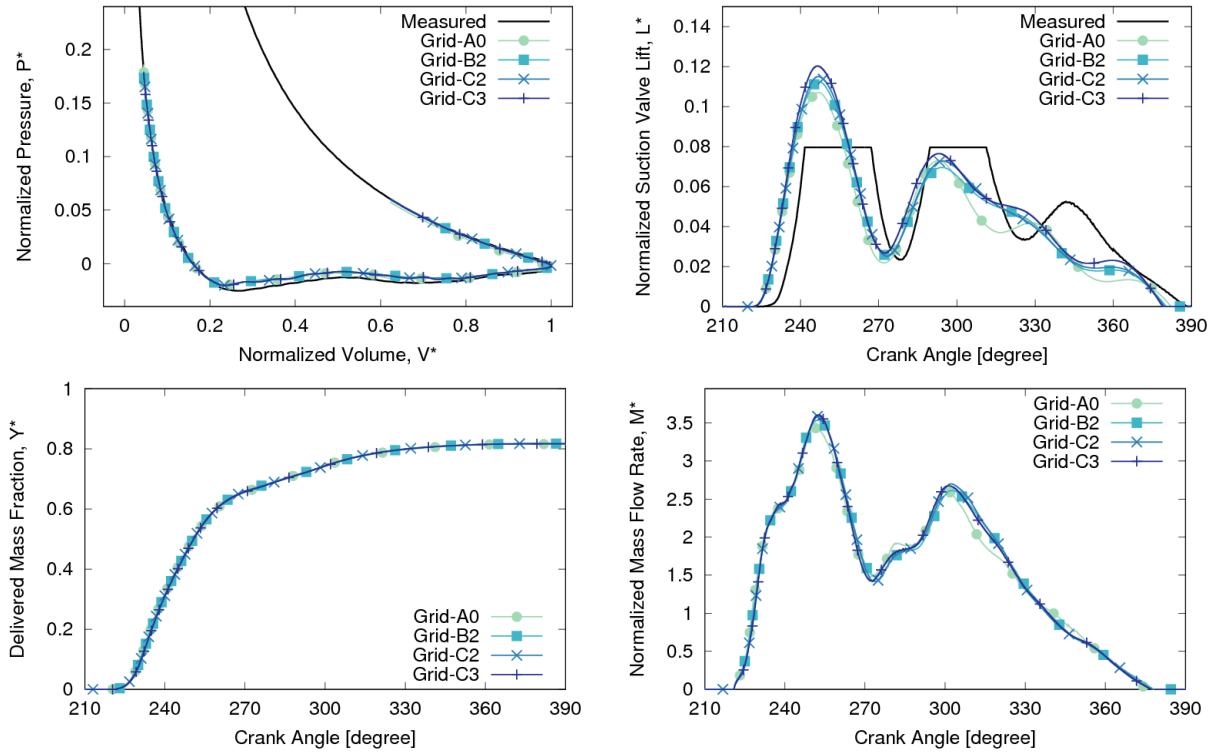

Figure 4: Calculated quantities during the suction process for four of the grids studied and experimental measurements. Top left shows the pressure vs. volume. Top right shows the suction reed lift, bottom left shows the delivered mass fraction, and bottom right shows the mass flow rate into the cylinder all as functions of crank angle.

The discharge process showed slightly more grid sensitivity than did the suction process. Figure 5 shows two representative cut-planes from during the discharge event. The bending of the reed valve and booster can be seen in these figures, as can the large amount of cells that are added adaptively near the valve opening. Figure 6 shows the PV diagram, discharge lift (normalized by the valve length), and Y* and M* evolution. The only real outlying point is the coarsest grid, Grid-A0, and the other grids indicate reasonable convergence of these quantities. The data from all grid convergence studies is summarized in Table 2.

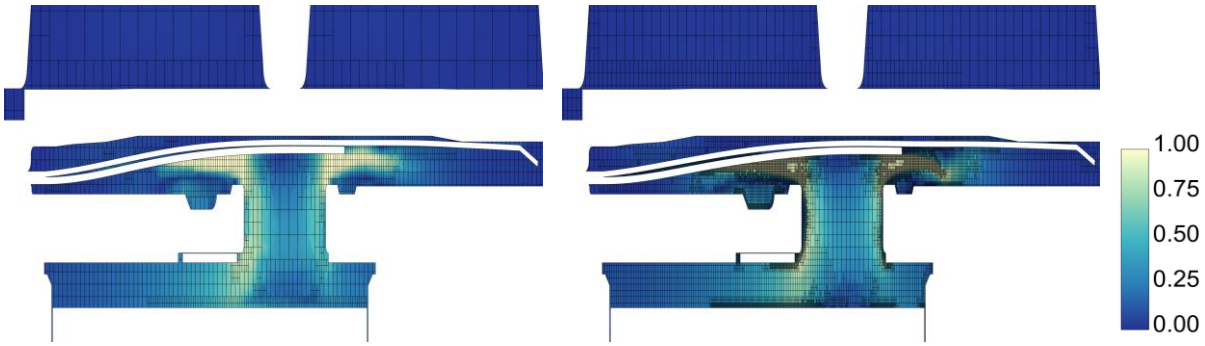

Figure 5: Cut-planes along the center of the discharge reed, colored by normalized velocity for two of the grids studied. The grids are Grid-B3 and Grid-C4 from left to right. The view is skewed to exaggerate the bending.

The results of the grid resolution studies for both suction and discharge events are summarized by Table 2. Global quantities of *Y** at the end of the cycle showed very little variation on any of the grids, save the coarsest Grid-A0. The maximum flow rate, *M**, showed slightly more variation, however, which does indicate important grid effects in resolving the temporally accurate and spatially accurate mass flow through the valves.

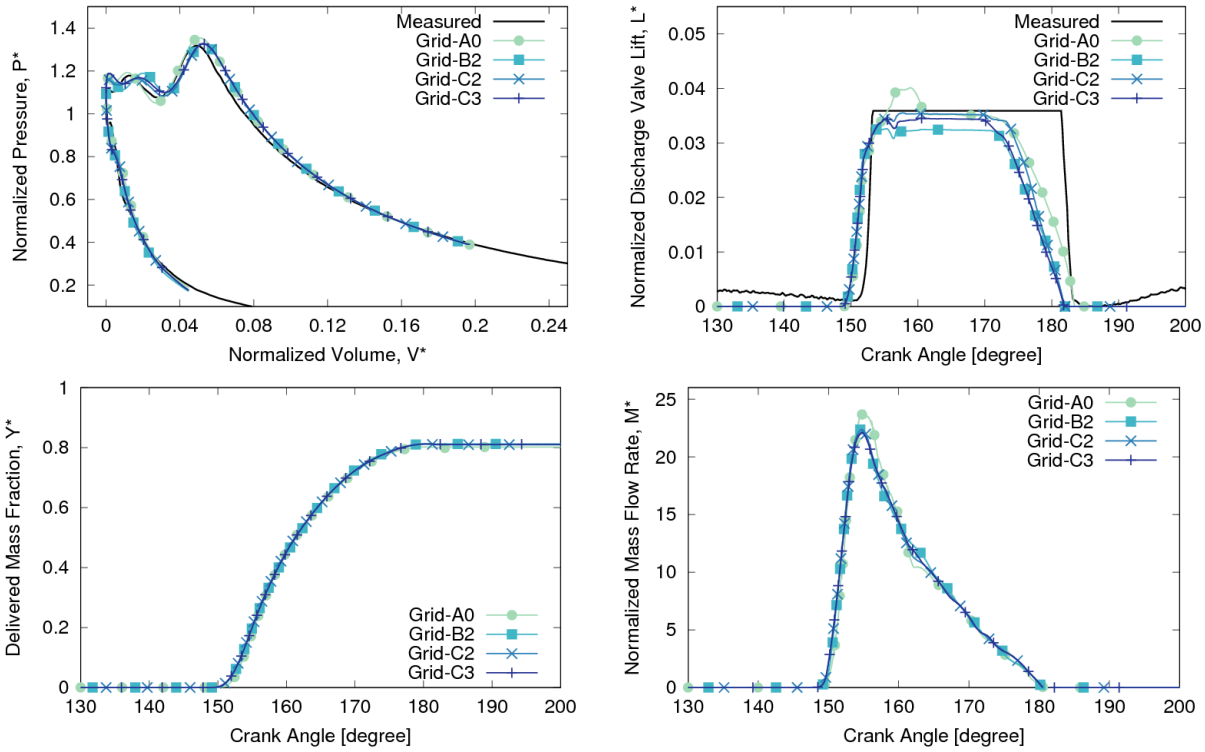

Figure 6: Calculated quantities during the discharge process for four of the grids studied and experimental measurements. Top left shows the pressure vs. volume. Top right shows the suction reed lift, bottom left shows the delivered mass fraction, and bottom right shows the mass flow rate into the cylinder all as functions of crank angle.

Table 2: Results from Grid Resolution Studies

	Suction				Discharge			
Grid Name	*Y**	**Max(*M**)**	**Wall Clock Time (hr)**	**CPU Time (core hr)**	*Y**	**Max(*M**)**	**Wall Clock Time (hr)**	**CPU Time (core hr)**
Grid-A0	0.816	3.43	0.9	3.6	0.802	23.9	0.5	2.1
Grid-B0	0.817	3.53	3.3	13	0.812	22.4	1.5	5.8
Grid-B2	0.817	3.54	5.0	20	0.812	22.4	4.0	16
Grid-B3	0.817	3.56	8.1	65	0.810	22.8	3.4	27
Grid-C2	0.817	3.59	10.2	163	0.810	22.4	3.7	58
Grid-C3	0.817	3.60	26.4	423	0.811	22.1	8.1	130
Grid-C4	0.817	3.57	73.8	1180	0.811	22.9	27.0	432

4.2 Effects of temporal discretization

As the grid is refined, the time-step also adjusts accordingly based on the imposed CFL restrictions. It is possible, however, to run the model at larger time steps by increasing the CFL number. If the CFL number becomes too large, there may be significant temporal error in the solution fields. Grid-C2 has been assessed at larger CFL numbers of 2.0 and 4.0. The results in Table 3 show measures for a complete cycle.

The suction process is virtually unaffected by running at larger time steps, however the discharge process shows slightly greater sensitivity, affecting the maximum pressure by around 2% when a CFL number as large as 4.0 is used. It is recommended, therefore, to allow a higher CFL number during suction. The tests show that a large improvement in run-time, near 50% savings, can be achieved by using the higher CFL numbers. The run-time improvement is very good from CFL of 1.0 to 2.0, but the improvement is marginal when CFL is increased to 4.0

due to the extra work required when solving each transport equation to the specified tolerance. The use of the biconjugate gradient stabilized method for solving the pressure equation greatly improves the method's ability to solve the pressure equation efficiently when the time step is large.

Table 3: Results from Temporal Resolution Studies on Grid-C2

Grid	CFL	Timesteps (per cycle)	Wall Time (hr/cycle)	Y*	Max(P*)
Grid-C2	1.0	13000	15.5	0.824	1.311
Grid-C2	2.0	6500	8.4	0.824	1.315
Grid-C2	4.0	3800	6.0	0.824	1.322

4.3 Effects of valve sealing model

The numerical modeling of the sealing of the valves is another important part of the model that must be scrutinized for its effect on the accuracy. When the valve lift at the center of the seat is below a user-specified threshold, the flow between the valve and port is treated as perfectly sealed. When this lift exceeds the threshold, flow passes freely through the valve opening. By default, this tolerance is set to be very small, at 10^{-8} m. If it is too small, the simulation may be expensive to due high velocities and small cells. If it is too large, the simulation will suffer from the numerical artifact of flow being restricted when the valve is open. Values of 10^{-8}, 10^{-7}, 10^{-6}, and 10^{-5} m are tested here and found to have negligible effect on the maximum flow rate and the total mass flow. In Figure 7 (a), the artifact caused by late opening is seen. Despite the small effect on the global statistics, it is recommended to use a small value around 10^{-8} to 10^{-7} m for this parameter, as the additional run time to the simulation is also small.

A second numerical effect in the valve modeling is the modeling the seat contact. The current approach carries the limitation that the surfaces describing the computational volume are not allowed to intersect. Therefore, where valves contact seats there exists a thin gap in the model. Gaps of 10^{-4}, 10^{-5}, and 10^{-6} m were investigated in this study. It was found that a gap of 10^{-5} m performed best. If the gap were too small, the time step restriction is quite severe; if the gap were too large, the flow areas were slightly over-estimated.

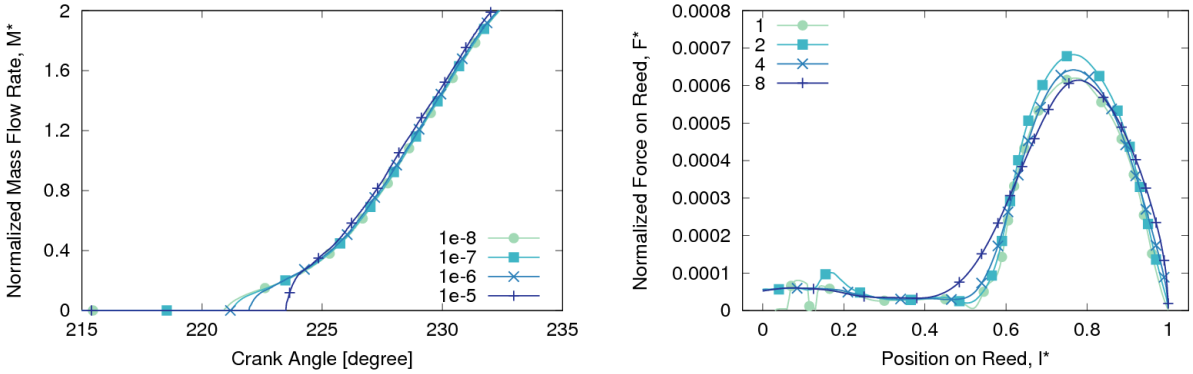

Figure 7: Mass flow right vs. crank angle (left) for varying lift openings, and pressure force along reed (right) for varying pressure window sizes.

4.4 Effects of pressure coupling between fluid and solid

The final numerical aspect of the model investigated here is the window size over which the pressure is evaluated on the solid beam. By default, a value equal to the base grid size is used. A tent function is employed to average the pressure from the fluid cells onto the beam. When the window size is increased, there may be a smearing of pressure data over the beam which can affect the motion. If the window size become two small, there may be nodes on the beam around which no fluid cell is close enough to evaluate. Figure 7 (b) shows how the normalized pressure force on the beam varies with window sizes of 1, 2, 4, and 8 factors of the base grid size. Because of the tent-function averaging, the smearing effect is somewhat reduced. There are no obvious changes to the model results over this range of variation of the pressure window.

6. CONCLUSIONS

In this study, we have investigated the numerical accuracy of applying a Cartesian cut-cell finite-volume method to reciprocating compressors. The method was found to be ideally suited to handling the moving complex geometries associated with the compressor tested. The numerical error showed that grid convergence can be achieved on relatively coarse grids, in part due to the small length scales and velocity scales in this problem. As the Reynolds number of the problem increases, the grid may show more sensitivity. Running at a higher CFL number, especially during the suction process, can significantly reduce the run time, with very minor effects on the accuracy. Recommended values for the valve height at which to open the flow and the gap to leave in the seat were reported. It is important to consider that the metrics used here for numerical convergence were primarily global quantities; there almost certainly more variation among the different grids when comparing local quantities. The numerical settings used in any calculation should be determined so that the main statistics of interest, whether they be global or local quantities, are sufficiently converged.

Overall, the amount of numerical uncertainties in the model were quite small compared to the difference between the experimental and model metrics of pressure and valve lift. This is demonstrative of two things: Firstly, the numerical technique applied in this work demonstrates numerical accuracy over the range of values tested; secondly, there is more uncertainty in the physical models themselves than in the numerics. Specifically, implementing realistic models for phenomena like leakage and stiction represent important physics which are lacking in the current model. There is considerable research effort devoted to these two topics already. The numerical method described here has been demonstrated as a platform in which these models could be tested further.

REFERENCES

Chikurde, R. C., Loganathan, E., Dandekar, D. P., Manivasagam, S. (2002). Thermal Mapping of Hermetically Sealed Compressors Using Computational Fluid Dynamics Technique. *Proceedings of the 16th International Compressor Engineering Conference at Purdue* (Paper 1520). West Lafayette, USA: Purdue University.

Cyklis, P. (1994). CFD Simulation of the Flow through Reciprocating Compressor Self-acting Valves. *Proceedings of the 12th International Compressor Engineering Conference at Purdue* (Paper 1016). West Lafayette, USA: Purdue University.

Fagotti, F., Possamai, F. C. (2000). Using Computational Fluid Dynamics as a Compressor Design Tool. *Proceedings of the 15th International Compressor Engineering Conference at Purdue* (Paper 1377). West Lafayette, USA: Purdue University.

Issa, R. I, (1985). Solution of the Implicitly Discretised Fluid Flow Equations by Operator-Splitting. *Journal of Computational Physics*, 62.

Karypis, G. (2013). A Software Package for Partitioning Unstructured Graphs, Partitioning Meshes and Computing Fill-Reducing Orderings of Sparse Matrices.

Kim, J., Wang, S., Park, S., Ryu, K., La, J. (2006). Valve Dynamic Analysis of a Hermetic Reciprocating Compressor. *Proceedings of the 18th International Compressor Engineering Conference at Purdue* (Paper 1805). West Lafayette, USA: Purdue University.

Mistry, H., Bhakta, A., Dhar, S., Bahadur, V., Dey, S. (2012). Capturing Valve Dynamics in Reciprocating Compressors through Computational Fluid Dynamics. *Proceedings of the 21st International Compressor Engineering Conference at Purdue* (Paper 1210). West Lafayette, USA: Purdue University.

Ottitsch, F. (2000). CFD: A Viable Engineering Tool for Compressor Valve Design or Just a Toy? *Proceedings of the 15th International Compressor Engineering Conference at Purdue* (Paper 1417). West Lafayette, USA: Purdue University.

Peng, D. Y. and Robinson, D. B. (1976). A New Two-Constant Equation of State. *Ind. Eng. Chem. Fund*., 15, 59-64.

Pereira, E.L.P, Deschamps, C.J., Ribas Jr., F.A. (2007). Performance analysis of reciprocating compressor through CFD simulation. *Proceedings of the International Conference on Compressors and their Systems* (pp. 310-318). London, England: City University of London.

Pereira, E.L.P, Deschamps, C.J., Ribas Jr., F.A. (2008). A comparative analysis of numerical simulation approaches for reciprocating compressor. *Proceedings of the 19th International Compressor Engineering Conference at Purdue* (Paper 1303). West Lafayette, USA: Purdue University.

Perkins, R.A., Laesecke; A., Ramires, M.L.V., Gurova, A.N., Cusco, L. (2000). Experimental thermal conductivity values for the IUPAC round-robin sample of 1,1,1,2-tetrafluoroethane (R134a), *NIST*, Gaithersburg, MD.

Poling, Prausnitz, O'Connell. (2001). The Properties of Gases and Liquids, 5th Ed., McGraw-Hill, p. 6.5.

Pomraning, E. (2000). Development of Large Eddy Simulation Models. *Ph.D. Dissertation, The University of Wisconsin-Madison*.

Pomraning, E., Richards, K., and Senecal, P. (2014). Modeling Turbulent Combustion Using a RANS Model, Detailed Chemistry, and Adaptive Mesh Refinement. *SAE Technical Paper* 2014-01-1116.

Prasad, B. G. (2004). CFD for Positive Displacement Compressors. *Proceedings of the 17th International Compressor Engineering Conference at Purdue* (Paper 1689). West Lafayette, USA: Purdue University.

Rhie, C. M. and Chow, W. L. (1983). Numerical Study of the Turbulent Flow Past an Airfoil with Trailing Edge Separation. *AIAA J*., 21, 1525-1532.

.

Rigola, J., Lehmkuhl, O., Ventosa, J., Pérez-Segarra, C.D., Oliva, A. (2012). Numerical simulation of the turbulent fluid flow through valves based on Low Mach models. *Proceedings of the 21st International Compressor Engineering Conference at Purdue* (Paper 1375). West Lafayette, USA: Purdue University.

Rodrigues, T. T., Da Silva, D. L. (2014). Turbulence Modelling Evaluation for Reciprocating Compressor Simulation. *Proceedings of the 22nd International Compressor Engineering Conference at Purdue* (Paper 2297). West Lafayette, USA: Purdue University.

Senecal, P. K., Pomraning, E., Richards, K. J., Briggs, T. E., Choi, C. Y., McDavid, R. M., Patterson, M. A., Hou, S., & Shethaji, T. (2007). A New Parallel Cut-Cell Cartesian CFD Code for Rapid Grid Generation Applied to In-Cylinder Diesel Engine Simulations. *SAE Technical Paper*, #2007-01-0159.

Tillner-Roth, R.; Baehr, H.D. (1994). An international standard formulation of the thermodynamic properties of 1,1,1,2-tetrafluoroethane (HFC-134a) covering temperatures from 170 K to 455 K at pressures up to 70 MPa. *J. Phys. Chem. Ref. Data*, 23, 5, 657-729.

Wang, Y., Krishan, K. and Dennin, M. (2007). Limits of the equivalence of time and ensemble averages in shear flows. *Phys. Rev. Lett.*, Vol. 98, Issue 22.

Yakhot, V. and Orszag, S. A. (1986). Renormalization Group Analysis of Turbulence. I. Basic Theory. *J. Sci. Comput.*, 1, 3.

ACKNOWLEDGEMENT

The authors acknowledge the support of Embraco for providing the compressor geometry, boundary conditions, and experimental data, as well as for their guidance in setting up and assessing the models.